ASME Journal of Engineering for Gas Turbines and Power
Online journal at:
https://asmedigitalcollection.asme.org/gasturbinespower

Sandra Megahed
Chair and Institute for Materials Technology,
Technical University of Darmstadt,
Grafenstrasse 2,
Darmstadt 64283, Germany

Erina Okabe
College of Science and Engineering,
Ritsumeikan University,
1-1-1 Nojihigashi, Kusatsu-shi,
Shiga 525-8577, Japan

Karl Michael Krämer[1]
Chair and Institute for Materials Technology,
Technical University of Darmstadt,
Grafenstrasse 2,
Darmstadt 64283, Germany
e-mail: michael.kraemer@tu-darmstadt.de

Christian Kontermann
Chair and Institute for Materials Technology,
Technical University of Darmstadt,
Grafenstrasse 2,
Darmstadt 64283, Germany

Christoph Heinze
Gas Services, Additive Manufacturing Technology,
Innovation and Digitalisation,
Siemens Energy Global GmbH & Co. KG,
Huttenstrasse 12,
Berlin 10553, Germany

Matthias Oechsner
Chair and Institute for Materials Technology,
Technical University of Darmstadt,
Grafenstrasse 2,
Darmstadt 64283, Germany

Creep Properties of Nickel Alloys—Comparison Between Conventional and Laser Powder Bed Fusion Manufacturing Routes

Metal laser powder bed fusion (PBF-LB/M) is a commonly used additive manufacturing process for gas turbine parts. This manufacturing method allows for small quantity batches with complex part designs. The mechanical behavior of PBF-LB/M components is strongly influenced by manufacturing process parameters, such as component geometry, build orientation, and postprocessing steps. However, these complex correlations are not completely understood—especially not for high-temperature applications. The number of publicly available publications on creep properties of nickel-based alloys is limited. This knowledge gap affects the design and qualification effort of PBF-LB/M gas turbine components. This study compares the creep properties of conventionally and additively manufactured IN738 LC and IN718. The assessment of PBF-LB/M additively manufactured samples includes experimental data from two types of specimens (witness and extracted samples) in three build orientations. Extracted samples out of additively manufactured components allow the investigation of application relevant mechanical properties. Build directions studied are 0 deg (perpendicular to build direction), 45 deg (diagonal), and 90 deg (parallel to build direction). The results show that the creep properties of PBF-LB/M manufactured IN738 LC at 850 °C are affected by build orientation. Samples oriented parallel to the build direction show favorable creep properties, especially 45 deg build orientations have reduced creep life properties. In comparison, the influence of build orientation is not as critical in IN718, and creep life properties at 650 °C are slightly superior to conventionally manufactured samples. [DOI: 10.1115/1.4068087]

Keywords: PBF-LB/M, IN738 LC, IN718, creep, generic test component, microstructure

Figure 1 defines the coordinate system used in this study and includes schematic sample locations.

1 Introduction

One of the most common application examples for high-temperature materials is turbine blades in a jet engine. The gas flow route within a typical jet engine can be broken down into the cold and hot sections. In the cold section, average temperatures ranging from ambient to 550 °C can be reached [1]. Components in the cold section can therefore be made of light weight high-strength titanium (Ti)-alloys. The hot section consists of the region from the combustion chamber to the exhaust nozzle exit. The materials used

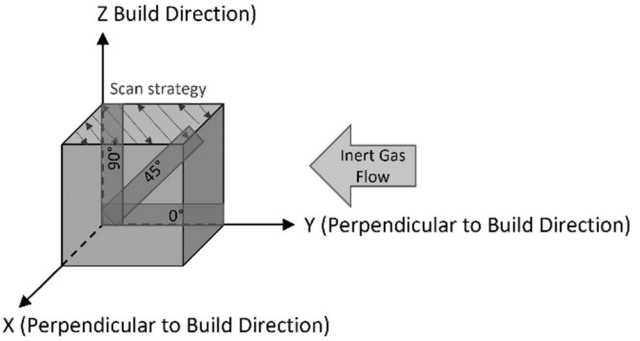

Fig. 1 Coordinate system used in this study and schematic sample locations

Turbo Expo, June 24–28, 2024. GT2024.
[1]Corresponding author.
Manuscript received November 14, 2024; final manuscript received February 28, 2025; published online April 7, 2025. Editor: Jerzy T. Sawicki.

in the combustion chamber and in the turbine must endure temperatures differences between 650 °C and 1250 °C [1].

The higher the turbine inlet temperature, the higher the achievable efficiency. It is therefore important to continue optimizing alloys to withstand even higher operating conditions. The lifetime of turbine components in the hot section is limited by the exposure duration to high thermal and mechanical stresses, repeated loading and environmental factors [2]. The expected lifetime for a conventionally manufactured (casting) blade in a stationary gas turbine until first revision is approximately 25,000 h [3].

Conventionally cast superalloys are limited in their design freedom and often contain porosity and cracking. These defects (i.e., porosity, cracks, etc.) act as crack initiation sites and hence limit the turbine blade lifetime [4].

Integrating conformal cooling channels can prolong the lifetime of components used in high-temperature applications by reducing the component temperatures. Metal laser powder bed fusion (PBF-LB/M) is a promising manufacturing route that allows for such innovate cooling concepts [5].

Metal laser powder bed fusion is a process in which thin layers of powder are deposited on a substrate and then selectively melted by a laser according to the sliced geometries of a three-dimensional computer-aided-design model [6–8].

IN738 LC is a γ'-precipitation strengthened nickel-based superalloy developed for turbine blades [9,10] with a maximum application temperature between 800 °C and 900 °C [10]. Research on manufacturing IN738 LC with PBF-LB/M began in 2013 and has since rapidly increased [11,12], but IN738 LC creep behavior remains largely unstudied.

IN718 is a precipitation strengthened Ni superalloy with good high-temperature strength and corrosion and oxidation resistance [13]. IN718 is characterized by very good weldability and is thus suited for processing by PBF-LB/M [14,15]. While the main strengthening phases (∼20 vol. % [16]), γ' and γ'', are beneficial to creep–rupture properties [17], once γ'' decomposes into the δ-phase between 650 °C and 980 °C, the mechanical properties, especially creep resistance, of IN718 decline significantly [18].

The PBF-LB/M microstructure is oriented; mostly parallel to build direction, which can be attributed to grains growing in the direction of the thermal gradient [19]. The resulting microstructure often presents a strong anisotropy, which affects mechanical short- and long-term properties [20–23].

Information about long-term creep behavior of conventional and PBF-LB/M is scarce in literature. This can be explained by the extensive experiments required for conventionally manufactured materials (e.g., casting, forging, etc.) combined with the many variations of PBF-LB/M process parameters, which have to be considered when designing the experiments (schematically shown in Fig. 2). Thus, the number of PBF-LB/M samples required for creep analysis increases significantly in comparison to conventional manufacturing.

In this study, a comparison of creep properties, such as creep-life and creep failure strains, between conventionally and PBF-LB/M processed IN738 LC is made to investigate general trends and influences of build direction and specimen types.

Experiments are conducted based on two types of specimens: Witness samples as defined by the standard DIN EN ISO/ASTM 52920 [24] and samples extracted from a demonstrator component. The samples are manufactured and extracted in three orientations: 0 deg (perpendicular to build direction), 45 deg (diagonal), and 90 deg (parallel to build direction).

2 Materials and Methods

2.1 Materials. The IN738 LC compositions for conventional and PBF-LB/M samples, as well as the nominal composition, are shown in Table 1. The IN718 compositions for conventional and PBF-LB/M samples, as well as the nominal composition, are shown in Table 2.

2.2 Sample Manufacturing. Since components used in high-temperature applications differ geometrically due to, e.g., sudden cross-sectional changes and/or undercuts, the creep behavior of witness samples and samples extracted from components are considered.

The witness samples were cylinders with $\varnothing 13 \times 80$ mm dimensions oriented in 0 deg, 45 deg, and 90 deg. The sample orientations are equivalent to the schematic in Fig. 1. The 0 deg and 45 deg samples were printed on supports to avoid build failure due to distortion of overhanging structures.

The conventionally manufactured IN738 LC samples were coarse grain cast, which is a common manufacturing route for turbine blade applications [4]. The grains obtained with this manufacturing route do not grow with a dominant grain orientation. Anisotropy is therefore not to be expected from these samples.

Metal laser powder bed fusion processing of IN738 LC was carried out with a volume energy density

$$\left(\frac{\text{Laser Power}}{\text{Layer Thickness} \times \text{Scan Speed} \times \text{Hatch Distance}}\right)$$

of 69 J/mm^3 and a layer thickness of 40 μm on an EOS M290 machine.

All samples (from both manufacturing routes) were thermally postprocessed prior to any mechanical testing and analysis. The first step of the postprocessing included a hot isostatic pressing. After hot isostatic pressing, further postprocessing was carried out as described by Messé et al. [27]:

- 2 h held at γ' solvus temperature ranging between 1120 and 1230 °C followed by air cooling.
- 24 h held at 850 °C followed by air cooling.
- During heat treatment, samples are exposed to an argon atmosphere to avoid oxidation.

The IN718 conventionally manufactured samples were forged. The PBF-LB/M samples were manufactured on an SLM280HL twin. The volume energy density used was 62 J/mm^3. No preheating was applied. After the PBF-LB/M process, all samples for mechanical testing were heat treated. A standardized IN718 heat treatment (AMS5663—see Fig. 3) similar to Refs. [28] and [29] was performed.

2.3 Tensile and Creep Testing. For tensile testing, a Zwick-Roell machine was used with a three-zone convection oven (max. temperature 1100 °C). Tensile tests were carried out according to DIN EN ISO 6892-1 [30]. All samples are machined into the final sample geometry, shown in Fig. 4. The tensile tests were carried out

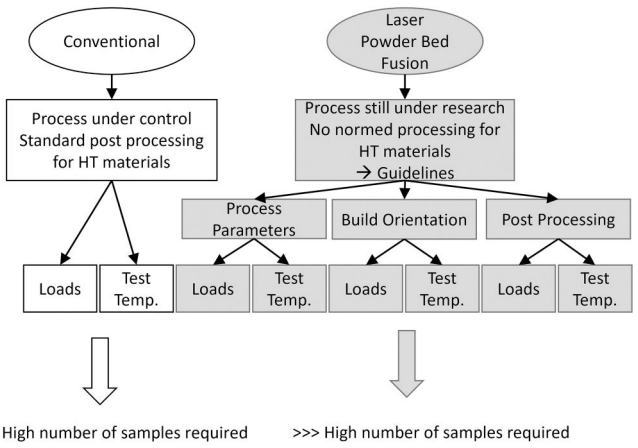

Fig. 2 Schematic representation of creep behavior analysis for conventional and PBF-LB/M samples

Table 1 IN738 LC compositions in wt. % for conventionally and PBF-LB/M manufactured samples as well as nominal composition

Conventional	Ni	C	B	Zr	Ta	Nb
	Balance	0.095	0.011	0.02	1.75	0.79
	Ti	Cr	Al	Co	Mo	W
	3.44	16.05	3.55	8.17	1.78	2.59
PBF-LB/M processing	Ni	C	B	Zr	Ta	Nb
	Balance	0.09	<0.015	0.081	1.9	0.9
	Ti	Cr	Al	Co	Mo	W
	3.4	15.8	3.5	9.1	1.78	2.6
Nominal range [25]	Ni	C	B	Zr	Ta	Nb
	Balance	0.09–0.13	0.007–0.012	0.03–0.08	1.5–2.0	0.6–1.1
	Ti	Cr	Al	Co	Mo	W
	3.2–3.7	15.7–16.3	3.2–3.7	3.0–9.0	1.5–2.0	2.4–2.8

Table 2 IN718 compositions in wt. % for conventionally and PBF-LB/M manufactured samples as well as nominal composition

Conventional	Ni	C	B	Zr	Ta	Nb
	Balance	0.05	<0.005	<0.01	<0.01	4.79
	Ti	Cr	Al	Co	Mo	W
	1.02	20.02	0.47	0.26	3.58	—
PBF-LB/M processing	Ni	C	B	Zr	Ta	Nb
	Balance	0.03	0.002	—	0.11	5.0
	Ti	Cr	Al	Co	Mo	W
	0.99	19.3	0.46	0.16	3.17	—
Nominal range [26]	Ni	C	B	Zr	Ta	Nb
	Balance	Max. 0.08	<0.01	—	Max. 0.05	4.75–5.5
	Ti	Cr	Al	Co	Mo	W
	0.65–1.15	17–21	0.2–0.8	Max. 1	2.8–3.3	—

at 850 °C. The strain rates lie between 0.5%/min (elastic regime) up to 5%/min (plastic regime).

Creep tests were carried out according to DIN EN ISO 204 [31] at 850 °C and 150–300 MPa for IN738 LC and at 650 °C for IN718 using a lever loaded single specimen test machine. Ceramic extensometers as well as three (3) type S thermocouples tied onto the sample surface were used. The sample geometry is the same as in Fig. 4.

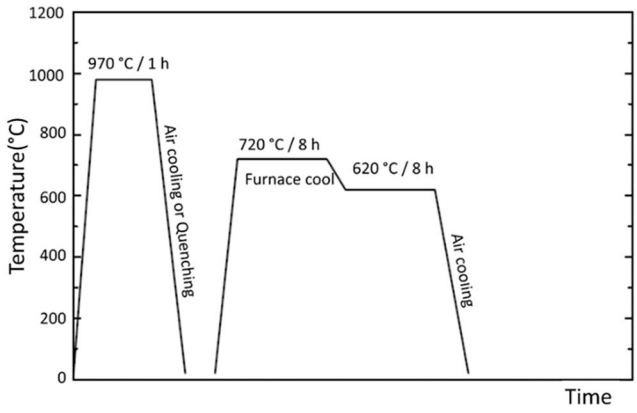

Fig. 3 AMS5663 heat treatment applied to IN718 samples

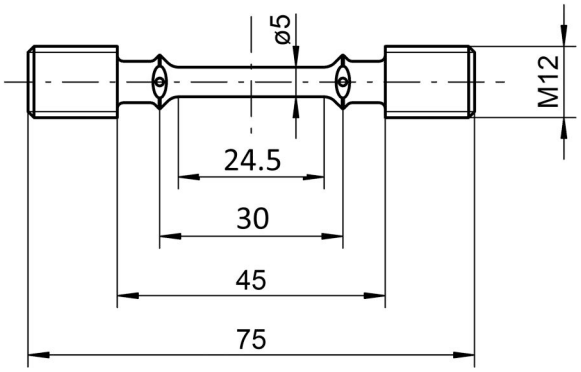

Fig. 4 Tensile and creep sample geometry

2.4 Microstructural Analysis. For microstructural investigations, metallographic specimens were prepared. The investigations were carried out on polished and etched (using V2A etchant) surfaces. The scanning electron microscopic (SEM) investigations were carried out on a Zeiss SEM microscope (Zeiss Auriga) with EDAX software.

Electron backscatter diffraction (EBSD) analysis was carried out in *XZ*-direction parallel to build direction to determine phase formation.

2.5 Thermo-Calc. Phase diagrams were calculated using Thermo-Calc2022a for the IN738 LC composition shown in Table 1. Scheil–Guliver and equilibrium solidification conditions were considered using the TCNI8 thermodynamic database [32].

3 Results and Discussion

As a first step in comparing conventional and PBF-LB/M witness samples, hot tensile tests were performed at 850 °C for IN738 LC. An overview of the IN738 LC tensile results ($R_{P0.2}$, ultimate tensile strength (UTS), and elongation Z) is shown in Table 3.

Based on literature [11,12], it is expected that the 90 deg build orientation shows the largest elongation but lower tensile and yield strengths (UTS and $R_{P0.2}$, respectively) compared to the 0 deg build

Table 3 Overview of IN738 LC tensile properties for conventionally and PBF-LB/M manufactured samples tested at 850 °C

		PBF-LB/M		
	Conventional	0 deg	45 deg	90 deg
$R_{P0.2}$ (MPa)	516	494	502	510
UTS (MPa)	722	727	719	740
Z (%)	11	21.9	21.9	24.5

Table 4 Overview of IN738 LC creep life results at 850 °C for conventionally cast and PBF-LB/M samples

	Applied stress (MPa)	Sample type	Build orientation (deg)	Time to rupture (h)	Creep failure strain (%)
Conventional	300	Extracted	—	150	6.6
	270	Extracted	—	422	7.8
	240	Extracted	—	1130	5.5
	210	Extracted	—	2039	5.0
	195	Extracted	—	3709	8.0
	160	Extracted	—	2626	2.2
PBF-LB/M	225	Witness	0	335	2.42
		Witness	45	194	2.78
		Witness	90	1342	5.27
		Extracted	0	309	1.65
		Extracted	45	171	2.38
		Extracted	90	2348	3.97
	200	Witness	0	912	1.72
		Witness	45	534	3.37
		Witness	90	5362	8.61
	180	Extracted	0	1684	1.89
		Extracted	45	651	1.65
	150	Witness	0	7983	2.47
		Witness	45	3636	3.25

direction. The 45 deg build orientation is expected to lie within the bounds of 0 deg and 90 deg build orientations. The results shown are comparable to those in literature [4,33] and correspond to the expectation regarding the PBF-LB/M build orientations.

The $R_{P0.2}$ and UTS values of the PBF-LB/M build orientations vary within 5%. Due to scatter, this difference is negligible. In terms of IN738 LC elongation, as expected, the 90 deg PBF-LB/M build orientation shows the largest elongation, since the tensile stresses are applied parallel to grain orientation. The columnar grains, oriented in build direction, are therefore capable of distributing the applied stresses evenly leading to larger elongation values. Comparatively, the 0 deg and 45 deg build orientations achieve only 21.9% elongation. Since the grains are either perpendicular or at a 45 deg angle to the applied tensile stresses, the grains are unable to distribute the applied stresses evenly leading to the reduced elongation values. The results are comparable to those reported in literature [34].

The IN738 LC $R_{P0.2}$ and UTS values of conventionally and PBF-LB/M manufactured samples are similar. However, the maximum elongation of conventionally manufactured IN738 LC samples is only about half of that of PBF-LB/M samples for all build orientations. This can be attributed to the casting process and relates to the typically large grain microstructure, which affects uniform plastic deformation, and casting process related defect formation such as porosity and internal cracking.

Since differences in tensile elongation behavior between conventionally and PBF-LB/M manufactured samples were found, differences in creep behavior are expected. To compare the creep life behavior of the PBF-LB/M samples, with the conventionally cast variants, a stress-life analysis using the time- and temperature-dependent Larson–Miller parameter (LMP) was performed. The data from a total of 263 creep experiments on conventionally cast samples in the temperature range of 550–1000 °C were collected from the LAMBDA high-temperature material database, administered by TU Darmstadt. The tests were performed in publicly and industry funded projects. A creep life master curve and a lower boundary curve, based on the 95%-confidence interval, were deducted from the data. For more information about scatter analysis of creep data, refer to Ref. [35].

The creep properties of conventionally manufactured and PBF-LB/M (and the respective build orientations) manufactured samples tested at 850 °C with similar load levels are of particular interest when assessing creep mechanisms. The base parameters of these tests are listed in Table 4. Only the 90 deg oriented PBF-LB/M samples reach times to rupture and creep failure strains in the same range as conventionally cast samples; however, witness samples seem to outlast extracted samples.

The 0 deg and 45 deg oriented PBF-LB/M samples, however, reach lower times to rupture and creep failure strains, which can be correlated to the microstructure [28,34,36]. Unexpectedly, the 45 deg build orientations reach the lowest times to rupture. Since, the 45 deg creep failure strains are between those of the 0 deg and 90 deg build orientations (see Table 4), the 45 deg time to rupture and hence creep rate must be correlated to the operating creep mechanisms. This material-specific behavior can be attributed with the precipitate structure formed in the PBF-LB/M process and is described in detail in Ref. [36].

This observation was also confirmed with a Larson–Miller plot (LMP versus stress) (see Fig. 5), which represents a parametric relation used to extrapolate experimental data on creep and rupture life.

As can be seen, the PBF-LB/M 90 deg build orientation lies above the master curve, which represents the data of the conventionally manufactured samples and therefore indicates that the 90 deg build orientation outperforms conventionally manufactured samples. The PBF-LB/M 45 deg build orientation concentrates at the lower boundary of the conventionally manufactured dataset and is therefore comparable to the worst-case scenario of conventional samples. The PBF-LB/M 0 deg build orientation lies within the bounds of the master curve and the lower boundary.

Regarding the creep behavior of the different build orientations of IN738 LC PBF-LB/M samples, publicly available literature can be

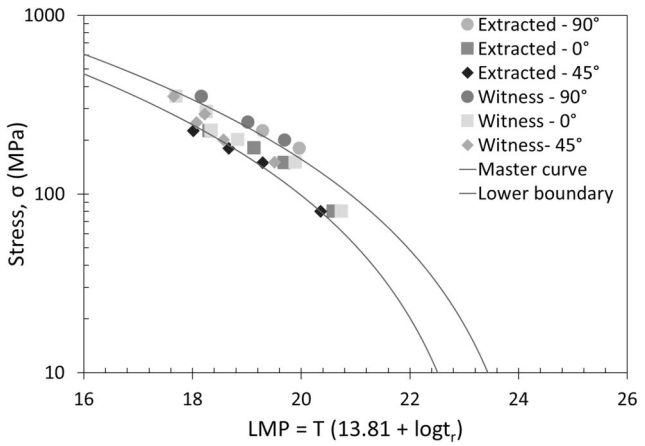

Fig. 5 Larson–Miller plot for witness and extracted IN738 LC PBF-LB/M samples. The master curve and lower boundary are based on conventionally manufactured IN738 LC samples.

found [11,34,36–39]. As seen in Fig. 5, the 45 deg build orientations show a significantly lower time to rupture and hence higher creep rate compared to the other two build orientations. Based on the trend of the creep failure strain, the time to rupture and creep rate is to be correlated to the creep mechanism.

The root cause of the difference in creep properties between the build orientations is traced back to the PBF-LB/M solidification conditions, leading to different creep mechanisms for each of the build orientations.

The solidification conditions determine not only grain size, grain orientation, and grain morphology but also phases formed. The main differences between PBF-LB/M and casting lie within the cooling rate. Whereas the cooling rates for casting can reach up to 1 K/s, the PBF-LB/M cooling rate lies roughly at 10^6 K/s [40]. Hence, PBF-LB/M solidification conditions are best modeled using Scheil–Gulliver assumptions [32]. For coarse-grained casting, equilibrium solidification conditions are considered.

Using Thermo-Calc, a phase diagram for both solidification conditions was obtained (Fig. 6). The predicted phases for both solidification conditions are listed in Table 5.

As can clearly be seen, the phases under the different solidification conditions differ significantly. Under Scheil–Gulliver conditions, σ, Laves, and tetragonal close packed (TCP) phases as well as the hexagonal close packed (hcp) phase η are predicted. For equilibrium, γ, γ', and various types of carbides are expected.

The microstructures for the conventionally cast sample tested at 850 °C and 240 MPa and the PBF-LB/M witness samples tested under the same conditions are shown in Fig. 7. Besides the obvious difference in grain size (conventional: ∼5 mm [4]; PBF-LB/M: ∼80 μm), differences regarding phase formation (as predicted by Thermo-Calc) can be identified.

While the conventionally manufactured samples achieve the creep properties by reducing the amount of grain boundaries and thereby increasing dislocation mobility, the creep properties of the PBF-LB/M manufactured samples are reached by carbides pinning the grain boundaries in the case of the 0 deg and 90 deg build orientation [34]. As shown in Table 5, the hcp η-phase is predicted under Scheil–Gulliver solidification conditions. The η-phase was found using EBSD analysis, however only within the 45 deg build orientation (see Fig. 8). For η-phase formation, carbides must dissolve when exposed to ∼850–950 °C for an extended period of time. Figure 8 confirms that the 45 deg build orientation does not contain carbides. The dissolution of carbides allows for grain boundary sliding leading to shorter times to rupture and faster creep rates within the 45 deg build orientation as seen in Fig. 5.

The reason for the η-phase only being present in the 45 deg build orientation can be found when considering the solidification conditions of the individual build orientations. As described in Sec. 2.2, the 0 deg and 45 deg build orientations were built on supports to avoid build failure due to distortion. With the use of supports, the contact area between sample and substrate plate (i.e., heat sink) increases compared to that of the 90 deg build orientation (contact area: 133 mm^2). The contact area of the 0 deg sample is the largest with 1500 mm^2. The 45 deg contact area lies within the bounds of the 0 deg and 90 deg build orientation, allowing for optimal thermal conditions for the η-phase to form.

Table 5 Phases predicted for IN738 LC by Thermo-Calc under Scheil and equilibrium solidification conditions

Scheil (represents PBF-LB/M)	Equilibrium (represents casting)
Liquid	Liquid
FCC_AL	MC
FCC_AL #2	FCC
Corundum	L_{12}_FCC
BCC_A2	M_7C_3
SIGMA	$M_{23}C_6$
MB_2_C_{32}	MB_2
ZrO_2_MONO	
Ni_3Ti	
G-Phase	
Laves_Phase_C_{14}	

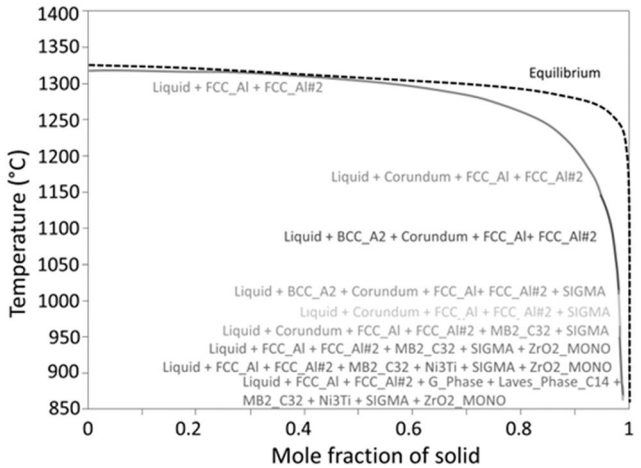

Fig. 6 Thermo-Calc phase diagram under Scheil and equilibrium solidification conditions

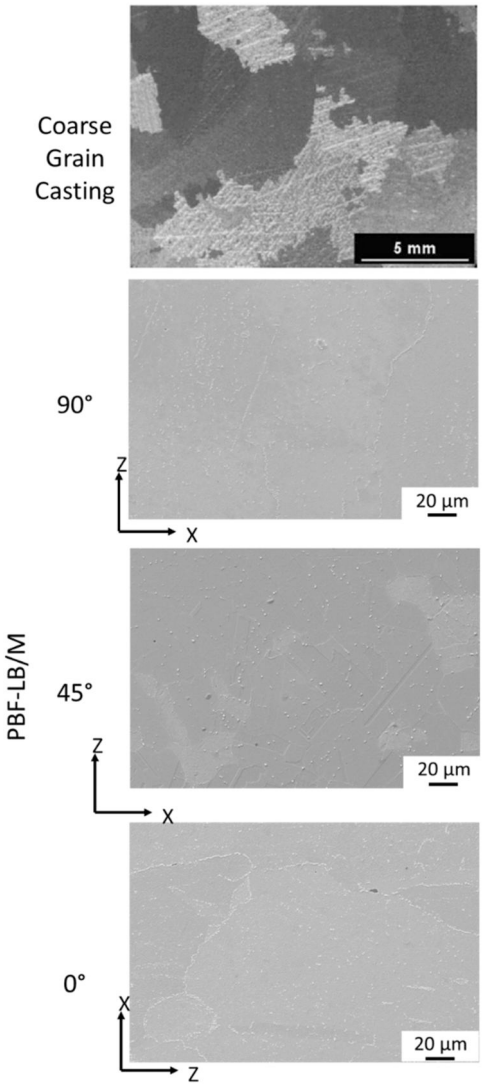

Fig. 7 Overview of IN738 LC microstructures for conventionally and PBF-LB/M manufactured witness samples

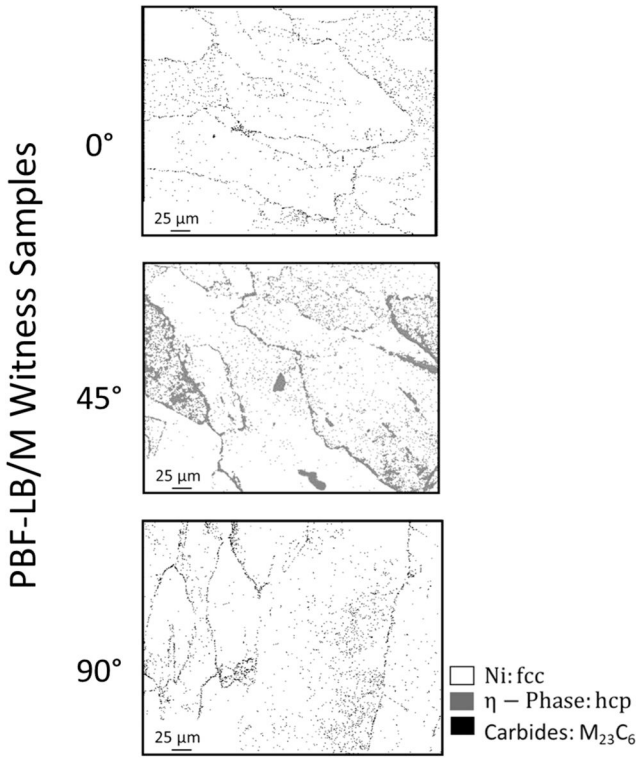

Fig. 8 PBF-LB/M IN738 LC EBSD-maps for phase identification. The different build orientations for the PBF-LB/M samples are considered.

The difference in creep mechanisms was also evaluated based on a Norton analysis. For a detailed description about the Norton plot, refer to Ref. [41]. Figure 9 shows a Norton plot for conventionally and PBF-LB/M samples without the distinction between the PBF-LB/M build orientations. From Fig. 9, it can be seen that while scatter is apparent for both manufacturing routes, the trend lines show an R^2 value of ∼0.7.

Also noticeable is that the gradient of the PBF-LB/M samples is similar to that of the gradient of the conventionally manufactured samples. The Norton stress exponents, which are represented by the gradient, for the PBF-LB/M samples lie at 5.7, while that of the conventionally manufactured samples lie at 6. The values of the stress components indicate that the expected dominant creep mechanism is dislocation creep (i.e., power law creep).

In order to also consider the influence of PBF-LB/M build orientations, Fig. 10 shows the same Norton plot, but with different symbols for all considered build orientations (namely, 0 deg, 45 deg, and 90 deg) in comparison to conventionally manufactured samples. As can be seen, the conventionally manufactured samples and the respective stress exponents are similar to that of the PBF-LB/M 90 deg build orientation (both witness and extracted). Therefore, the dominant expected creep deformation mechanism for conventionally manufactured samples and the PBF-LB/M 90 deg build orientation is dislocation creep. The stress exponent of the 0 deg PBF-LB/M samples (both witness and extracted) are comparatively lower at ∼4.4, meaning that a mixture of dislocation creep and grain boundary sliding is expected. The lowest stress exponents are shown by the 45 deg PBF-LB/M samples (both witness and extracted). Therefore, while dislocation creep may occur, this is no longer the dominant creep deformation mechanisms within the 45 deg build orientation, but rather diffusion-based creep deformations are dominant.

Regarding the IN738 LC results, it can be conclusively said that while the PBF-LB/M creep properties are comparable to those of conventionally manufactured samples, the creep deformation mechanisms differ. The PBF-LB/M 90 deg build orientation and the conventionally manufactured samples show similar times to rupture, creep failure strains, and stress exponents, indicating similar dominant creep deformation mechanisms. The 45 deg and 0 deg PBF-LB/M build orientations, on the other hand, show inferior times to rupture, creep failure strains (while still within the lower boundary of conventionally manufactured samples), and lower stress exponents, indicating that there are other dominant creep mechanisms to be expected for these build orientations.

To assess, if the findings regarding the similarity of the creep results between conventional and PBF-LB/M samples can be transferred to other nickel superalloys, LMP- and Norton plots for IN718 were determined. The conventional database consists of 67 tests performed in the temperature range of 500–1000 °C. The tests on PBF-LB/M samples were conducted at 650 °C. Figure 11 shows the IN718 Larson–Miller plot.

It can be seen that similar to the IN738 LC results discussed above, the PBF-LB/M IN718 creep results can outperform the conventionally manufactured samples under certain conditions.

Similar to IN738 LC, a Norton plot was analyzed to predict the expected dominant creep mechanism. The Norton plot for PBF-LB/M and conventionally manufactured samples is shown in Fig. 12. The reliability of the data can be deduced from the R^2 values. Both the PBF-LB/M and conventional line show R^2 values above 0.99.

The gradient of the lines (i.e., the stress exponent) can be deduced. The PBF-LB/M samples show a stress exponent of 8.6, while the conventionally manufactured samples show a stress exponent of 8.2. Both stress exponents indicate an expected dominant creep deformation mechanism of dislocation creep (i.e., power law creep).

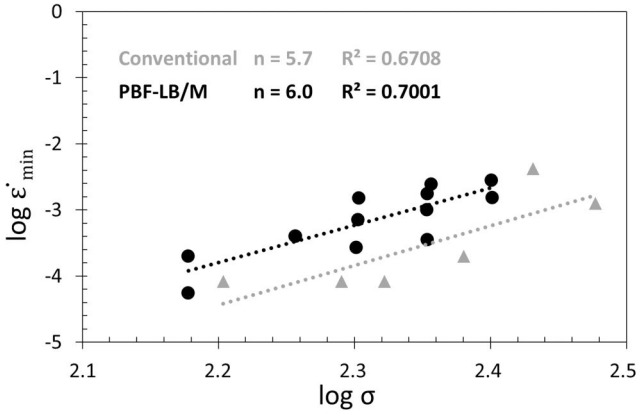

Fig. 9 Norton plot for IN738 LC PBF-LB/M samples in comparison to conventionally manufactured samples at 850 °C

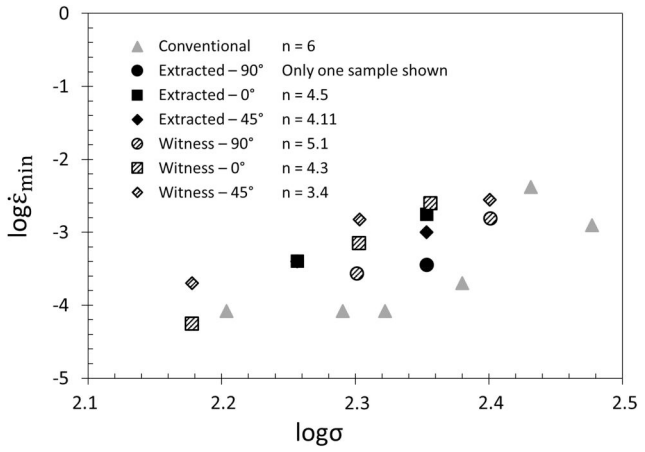

Fig. 10 Norton plot for witness and extracted IN738 LC PBF-LB/M samples at 850 °C. The different build orientations are also considered.

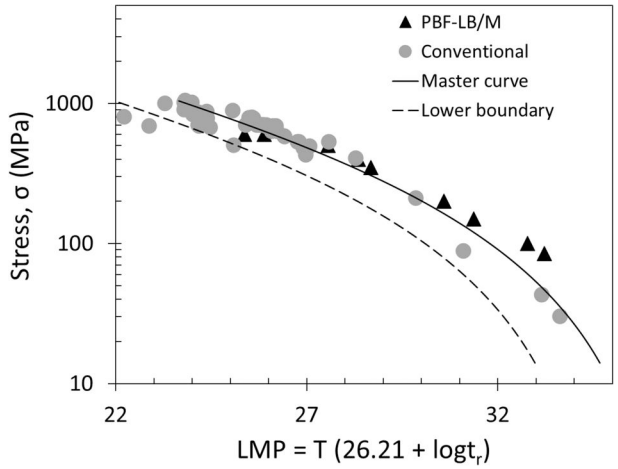

Fig. 11 Larson–Miller plot for conventional and PBF-LB/M IN718 samples. The master curve and lower boundary are based on conventionally manufactured IN718 samples. PBF-LB/M data at 650 °C.

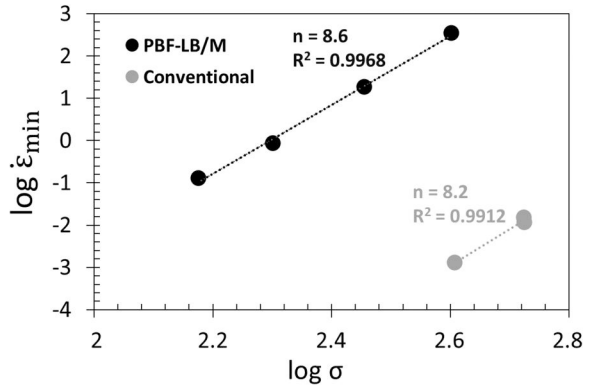

Fig. 12 Norton plot IN718 PBF-LB/M samples in comparison to conventionally manufactured IN718 samples at 650 °C

As concluded for IN738 LC, the IN718 PBF-LB/M creep properties are comparable to those of conventionally manufactured samples. As confirmed in literature and with stress exponents within this study, the expected dominant creep deformation mechanisms are identical for conventionally and PBF-LB/M manufactured IN718 samples (and all respective build orientations).

4 Conclusion

In this study, IN718 and IN738 LC PBF-LB/M witness and extracted samples are within measured scatter of conventionally manufactured samples in terms of creep behavior.

Different build orientations lead to different solidification conditions and creep mechanisms. The following conclusions can be drawn from this study:

- Comparing PBF-LB/M extracted samples and witness samples, the time to rupture of extracted samples, representing component-near build conditions, is shorter than that observed in witness samples. However, the creep property characteristics are comparable.
- From a creep life assessment via LMP, the PBF-LB/M 90 deg-build direction performs similarly to the mean of conventional material batch. The 0 deg and 45 deg build orientations are within the lower boundary of scattering.
- By assessing the minimum creep rates of IN738 LC at 850 °C via Norton plots, a change in dominating creep mechanism between build orientations and conventional materials is expected.
- By assessing the minimum creep rates of IN718 at 650 °C via Norton plots, a change in dominating creep mechanism between build orientations and conventional materials is not expected.

Even though the solidification conditions of the manufacturing routes of conventionally and PBF-LB/M manufactured samples differ significantly, the creep properties for IN738 LC as well as for IN718 were shown to be comparable or in the case of 90 deg orientation even outperform conventional variants. This can be correlated to the microstructures. While the conventional microstructures are optimized with regards to grain size and grain boundary area, the PBF-LB/M microstructure contains strengthening and grain boundary pinning phases that allow creep properties similar to or better than those of conventional samples to be reached. However, close attention to the build orientation must be taken during production planning. In order to produce components, e.g., gas turbine blades, with superior quality, the solidification conditions of the 90 deg build orientation need to dominate during the build process.

Acknowledgment

The research project (FVV Project No. 1401) was performed by the Institute of Materials Technology of the Technical University Darmstadt under the guidance of Professor Dr.-Ing. Matthias Oechsner and by the Materials Testing Institute at the University of Stuttgart under the guidance of Professor Dr.-Ing. Stefan Weihe. Based on a decision taken by the German Bundestag, it was supported by the Federal Ministry for Economic Affairs and Climate Action (BMWK) and the AIF (German Federation of Industrial Research Associations eV) within the framework of the industrial collective research (IGF) programme (IGF No. 21220 N/1). The authors gratefully acknowledge the support received from the funding organisations, from the FVV eV, and from all those involved in the project.

Funding Data

- FVV eV (Funder ID: 10.13039/501100003162).
- Federal Ministry for Economic Affairs and Climate Action (BMWK) and AIF (German Federation of Industrial Research Associations eV) within the framework of the industrial collective research (IGF) programme (IGF No. 21220 N/1; Funder ID: 10.13039/501100002723).

Data Availability Statement

The datasets generated and supporting the findings of this article are obtainable from the corresponding author upon reasonable request.

Nomenclature

E_V = volume energy density
EBSD = electron backscatter diffraction
hcp = hexagonal close packed
LMP = Larson–Miller parameter
PBF-LB/M = metal laser powder bed fusion
$R_{P0.2}$ = yield stress in MPa
t = time to rupture in seconds (s)
UTS = ultimate tensile strength in MPa
wt. % = weight percent
$\dot{\varepsilon}$ = minimal creep rate
ε_f = creep failure strain
σ = applied stress

References

[1] Rolls-Royce Ltd. and Rolls-Royce plc, 2015, *The Jet Engine*, Wiley, Chichester, West Sussex, UK.

[2] Farhat, H., 2021, "Lifetime Extension: Assessment and Considerations," *Operation, Maintenance, and Repair of Land-Based Gas Turbines*, Elsevier, Amsterdam, The Netherlands, pp. 175–196.
[3] Song, P., 2011, "Influence of Material and Testing Parameters on the Lifetime of TBC Systems With MCrAlY and NiPtAl Bondcoats: Fachgruppe für Metallurgie und Werkstofftechnik/Lehrstuhl für Werkstoffe der Energietechnik (FZ Jülich)/Lehrstuhl für Werkstoffchemie," Dissertation, Publikationsserver der RWTH Aachen University, Techn. Hochsch., Aachen, Germany.
[4] Mueller, F., Scholz, A., and Berger, C., 2011, "Creep Crack Behaviour of a Coarse Grain Nickel-Base Super Alloy," Mater. High Temp., **28**(2), pp. 103–108.
[5] Carter, L. N., 2013, "Selective Laser Melting of Nickel Superalloys for High Temperature Applications," Ph.D. thesis, School for Metallurgy and Materials, University of Birmingham, Birmingham, UK.
[6] ISO, 2016, "Additive Manufacturing—General Principles—Part 3: Main Characteristics and Corresponding Test Methods (ISO 17296-3:2014)," International Organization for Standardization, Geneva, Switzerland, Standard No. DIN EN ISO 17296-3:2016-12.
[7] ISO, 2016, "Additive Manufacturing—General Principles—Part 4: Overview of Data Processing (ISO 17296-4:2014)," International Organization for Standardization, Geneva, Switzerland, Standard No. DIN EN ISO 17296-4:2016-12.
[8] ISO, 2022, "Additive Manufacturing—General Principles—Fundamentals and Vocabulary (ISO/ASTM 52900:2021)," International Organization for Standardization, Geneva, Switzerland, Standard No. DIN EN ISO/ASTM 52900:2022-03.
[9] Bieber, C. G., and Galka, J. J., 1967, "Cast Nickel-Base Alloy," Huntington Alloys Corp, Huntington, WV, U.S. Patent No. 3459545 A.
[10] Sims, C., 1984, "A History of Superalloy Metallurgy for Superalloy Metallurgists," Superalloys, Schenectady, NY, pp. 399–419.
[11] Rickenbacher, L., Etter, T., Hövel, S., and Wegener, K., 2013, "High Temperature Material Properties of IN738 LC Processed by Selective Laser Melting (SLM) Technology," Rapid Prototyping J., **19**(4), pp. 282–290.
[12] Sanchez, S., Smith, P., Xu, Z., Gaspard, G., Hyde, C. J., Wits, W. W., Ashcroft, I. A., Chen, H., and Clare, A. T., 2021, "Powder Bed Fusion of Nickel-Based Superalloys: A Review," Int. J. Mach. Tools Manuf., **165**, p. 103729.
[13] Huan, Q. I., 2012, "Review of INCONEL 718 Alloy: Its History, Properties, Processing and Developing Substitutes," J. Mater. Eng., **2**(8), pp. 92–100.
[14] Henderson, M. B., Arrell, D., Larsson, R., Heobel, M., and Marchant, G., 2004, "Nickel Based Superalloy Welding Practices for Industrial Gas Turbine Applications," Sci. Technol. Weld. Joining, **9**(1), pp. 13–21.
[15] Helmer, H. E., Körner, C., and Singer, R. F., 2014, "Additive Manufacturing of Nickel-Based Superalloy Inconel 718 by Selective Electron Beam Melting: Processing Window and Microstructure," J. Mater. Res., **29**(17), pp. 1987–1996.
[16] Rösler, J., Hentrich, T., and Gehrmann, B., 2019, "On the Development Concept for a New 718-Type Superalloy With Improved Temperature Capability," Metals, **9**(10), p. 1130.
[17] Sanchez, S., Gaspard, G., Hyde, C. J., Ashcroft, I. A., Ravi, G. A., and Clare, A. T., 2021, "The Creep Behaviour of Nickel Alloy 718 Manufactured by Laser Powder Bed Fusion," Mater. Des., **204**(Part 2), p. 109647.
[18] Geddes, B., Leon, H., and Huang, X., 2010, *Superalloys: Alloying and Performance*, ASM International, Materials Park, OH.
[19] Wei, H. L., Mazumder, J., and DebRoy, T., 2015, "Evolution of Solidification Texture During Additive Manufacturing," Sci. Rep., **5**(1), p. 16446.
[20] Brune, T., Schueckler, P., Krämer, K. M., Kontermann, C., and Oechsner, M., 2020, "Mechanische Kurz- und Langzeiteigenschaften von additiv Hergestellten Bauteilen für den Hochtemperatureinsatz am Beispiel der Legierung IN718," Langzeitverhalten warmfester Stähle und Hochtemperaturwerkstoffe: Neues aus Anwendung und Forschung 43, Vortragsveranstaltung, Online-Konferenz Tagungsband, Forschungsvereinigung für Warmfeste Stähle und Hochtemperaturwerkstoffe, Düsseldorf, Germany, Nov. 27, pp. 1–13.
[21] Mohsin Raza, M., and Lo, Y.-L., 2021, "Experimental Investigation Into Microstructure, Mechanical Properties, and Cracking Mechanism of IN713 LC Processed by Laser Powder Bed Fusion," Mater. Sci. Eng.: A, **819**(12), p. 141527.
[22] Bridges, A., Shingledecker, J., Clark, J., and Crudden, D., 2023, "Creep Analysis and Microstructural Evaluation of a Novel Additively Manufactured Nickel-Base Superalloy (ABD®-900AM)," ASME J. Eng. Gas Turbines Power, **145**(6), p. 061005.
[23] Bridges, A., Shingledecker, J., Torkaman, A., and Houck, L., 2020, "Metallurgical Evaluation of an Additively Manufactured Nickel-Base Superalloy for Gas Turbine Guide Vanes," ASME Paper No. GT2020-14808.
[24] ISO, 2021, "Additive Manufacturing—Qualification Principles—Requirements for Industrial Additive Manufacturing Sites (ISO/ASTM DIS 52920:2021)," International Organization for Standardization, Geneva, Switzerland, Standard No. DIN EN ISO/ASTM 52920:2021-08.
[25] Inco, The Internactional Nickel Company, Inc., 2020, "Alloy IN-738 Technical Data," Inco, Durham, NC, accessed Mar. 28, 2025, https://nickelinstitute.org/media/4690/ni_inco_497_alloy738.pdf
[26] ASTM, 2023, "Specification for Precipitation-Hardening and Cold Worked Nickel Alloy Bars, Forgings, and Forging Stock for Moderate or High Temperature Service," ASTM, West Conshohocken, PA, Standard No. ASTM B637.
[27] Messé, O., Muñoz-Moreno, R., Illston, T., Baker, S., and Stone, H. J., 2018, "Metastable Carbides and Their Impact on Recrystallisation in IN738 LC Processed by Selective Laser Melting," Addit. Manuf., **22**, pp. 394–404.
[28] Sanchez, S., Hyde, C. J., Ashcroft, I. A., Ravi, G. A., and Clare, A. T., 2021, "Multi-Laser Scan Strategies for Enhancing Creep Performance in LPBF," Addit. Manuf., **41**(11), p. 101948.
[29] AMS F Corrosion and Heat Resistant Alloys Committee, 2016, "Nickel Alloy, Corrosion- and Heat-Resistant, Bars, Forgings, Rings, and Stock for Forgings and Rings, 52.5Ni–19Cr–3.0Mo–5.1Cb (Nb)–0.90Ti–0.50AI–18Fe, Consumable Electrode or Vacuum Induction Melted, 1775 ° F (968 °C) Solution Heat Treated, Precipitation-Hardenable," SAE Paper No. AMS5662N.
[30] ISO, 2019, "Metallic Materials—Tensile Testing (ISO 6892-1:2019)," International Organization for Standardization, Geneva, Switzerland, Standard No. DIN EN ISO 6892 1.
[31] ISO, 2019, "Metallic Materials—Uniaxial Creep Testing in Tension—Method of Test (ISO 204:2018)," International Organization for Standardization, Geneva, Switzerland, Standard No. DIN EN ISO 204:2019-04.
[32] Porter, D. A., and Easterling, K. E., 1997, *Phase Transformations in Metals and Alloys*, 2nd ed., Chapman & Hall, London/Weinheim, Germany.
[33] Wang, H., Zhang, X., Wang, G. B., Shen, J., Zhang, G. Q., Li, Y. P., and Yan, M., 2019, "Selective Laser Melting of the Hard-to-Weld IN738 LC Superalloy: Efforts to Mitigate Defects and the Resultant Microstructural and Mechanical Properties," J. Alloys Compd., **807**(11), p. 151662.
[34] Megahed, S., Krämer, K. M., Heinze, C., Kontermann, C., Udoh, A., Weihe, S., and Oechsner, M., 2023, "Influence of Build Orientation on the Creep Behavior of IN738 LC Manufactured With Laser Powder Bed Fusion," Mater. Sci. Eng.: A, **878**, p. 145197.
[35] Linn, S., Scholz, A., Oechsner, M., Berger, C., and Luesebrink, O., 2011, "Evaluation of Property Scatter of Ni-Base Alloy in 738 LC," Mater. Sci. Eng.: A, **528**(13–14), pp. 4676–4682.
[36] Megahed, S., Krämer, K. M., Kontermann, C., Heinze, C., Udoh, A., Weihe, S., and Oechsner, M., 2023, "Micro-Twinning in IN738 LC Manufactured With Laser Powder Bed Fusion," Materials, **16**(17), p. 5918.
[37] Megahed, S., Krämer, K. M., Heinze, C., Kontermann, C., Udoh, A., Weihe, S., and Oechsner, M., 2024, "Creep of IN738 LC Manufactured With Laser Powder Bed Fusion: Effect of Build Orientation and Twinning," Mater. High Temp., **41**(1), pp. 95–105.
[38] Risse, J., 2019, "Additive Fertigung der Nickelbasis-Superlegierung IN738 LC mittels selektivem Laserstrahlschmelzen," Dissertation, RWTH Aachen University, Aachen, Germany.
[39] Kunze, K., Etter, T., Grässlin, J., and Shklover, V., 2015, "Texture, Anisotropy in Microstructure and Mechanical Properties of IN738 LC Alloy Processed by Selective Laser Melting (SLM)," Mater. Sci. Eng.: A, **620**, pp. 213–222.
[40] Körner, C., Attar, E., and Heinl, P., 2011, "Mesoscopic Simulation of Selective Beam Melting Processes," J. Mater. Process. Technol., **211**(6), pp. 978–987.
[41] Norton, F. H., 1929, *The Creep of Steel at High Temperatures*, McGraw-Hill Book Company, New York.